Wet-surface–enhanced ellipsometric contrast microscopy identifies slime as a major adhesion factor during bacterial surface motility

Adrien Ducret[a,1], Marie-Pierre Valignat[b,1], Fabrice Mouhamar[a], Tâm Mignot[a,2], and Olivier Theodoly[b,2]

[a]Laboratoire de Chimie Bactérienne, Centre National de la Recherche Scientifique Unité Mixte de Recherche 7283, Institut de Microbiologie de la Méditerranée, Aix-Marseille University, 13402 Marseille cedex 20, France; and [b]Laboratory Adhesion & Inflammation, Institut National de la Santé et de la Recherche Médicale Unité Mixte de Recherche 1067, Centre National de la Recherche Scientifique Unité Mixte de Recherche 7333, Aix-Marseille University, 13402 Marseille cedex 20, France

Edited by Caroline S. Harwood, University of Washington, Seattle, WA, and approved May 3, 2012 (received for review December 20, 2011)

In biology, the extracellular matrix (ECM) promotes both cell adhesion and specific recognition, which is essential for central developmental processes in both eukaryotes and prokaryotes. However, live studies of the dynamic interactions between cells and the ECM, for example during motility, have been greatly impaired by imaging limitations: mostly the ability to observe the ECM at high resolution in absence of specific staining by live microscopy. To solve this problem, we developed a unique technique, wet-surface enhanced ellipsometry contrast (Wet-SEEC), which magnifies the contrast of transparent organic materials deposited on a substrate (called Wet-surf) with exquisite sensitivity. We show that Wet-SEEC allows both the observation of unprocessed nanofilms as low as 0.2 nm thick and their accurate 3D topographic reconstructions, directly by standard light microscopy. We next used Wet-SEEC to image slime secretion, a poorly defined property of many prokaryotic and eukaryotic organisms that move across solid surfaces in absence of obvious extracellular appendages (gliding). Using combined Wet-SEEC and fluorescent-staining experiments, we observed slime deposition by gliding *Myxococcus xanthus* cells at unprecedented resolution. Altogether, the results revealed that in this bacterium, slime associates preferentially with the outermost components of the motility machinery and promotes its adhesion to the substrate on the ventral side of the cell. Strikingly, analogous roles have been proposed for the extracellular proteoglycans of gliding diatoms and apicomplexa, suggesting that slime deposition is a general means for gliding organisms to adhere and move over surfaces.

label-free imaging | microfluidic

In mammals, cell migrations are essential for many developmental processes, for example during embryogenesis when the neural crest is formed and also during pathologies at the onset of the immune response or cancer metastasis (1). In these processes, the extracellular matrix (ECM) provides support and anchorage for cells, allowing local tissue differentiation and regulating intercellular communications (1). In general the ECM has a complex composition of polysaccharide gels (glycosaminoglycans) and fibrous proteins. Cells move along the ECM through focal adhesions and specific recognition of ECM components. In bacteria, the ECM also promotes extracellular recognition, adhesion, and motility, allowing the formation of antibiotic-resistant biofilms (2). Therefore, functional studies of the ECM have received attention in many fields from cancer biology to bacteriology.

Historically, electron microscopy has been the method of choice to image the structure of the ECM at high resolution. However, this method requires fixation procedures and does not allow studies of the ECM under live conditions. In general, live imaging approaches have used optical fluorescence microscopy and specific stains (i.e., antibodies, lectins) to localize specific components of the ECM, a polysaccharide or a given protein. A major limitation with these approaches is that they only allow the study of a selected ECM component and often interfere with function.

If optical microscopy remains the standard method to observe live microorganisms, novel approaches are required to image the ECM at high resolution with minimum specimen processing. However, in visible light, the ECM is generally invisible because thin ECM layers of organic translucent material have extremely low optical contrast. Thus, ECM detection is more a problem of contrast optimization than a problem of size magnification and lateral resolution. Different strategies have already been developed to enhance contrast and improve specimen visibility in optical microscopy. These strategies build on the fact that contrast is larger on a darker background for a given intensity difference. In fluorescence microscopy, the background is lowered by separating illumination and emission light with a spectral emission filter but this method requires labeling. In differential interference contrast (DIC) and phase-contrast microscopy, contrast enhancement of a transparent and unstained specimen consists in transforming phase changes induced by the specimen into intensity differences (3, 4). These techniques are efficient to visualize microscopic details of living cells and sometimes, internal organelles. However, the phase change induced by nanoscopic transparent objects is not sufficient for detection. Hence, there is no existing optical microscopy technique to detect immersed label-free thin films of organic materials with a thickness below 10 nm. In this context, we developed a unique optical microscopy method, which we called surface enhanced ellipsometric contrast microscopy in wet condition (Wet-SEEC), to image and quantify nanometer scale thin films on transparent substrates in solutions. The enhancement of optical contrast is based on specially designed substrate coatings in which multiple reflections and interferences yield dark background and very high contrast sensitivity to thin deposits. This unique technique makes possible the detection and measurement of molecular layers with a standard optical microscope, simultaneous to normal live wide-field imaging of microorganism. In particular, we show that Wet-SEEC can be used to image the ECM laid by migrating keratinocytes at unprecedented resolution.

In this report, we further took advantage of this Wet-SEEC method to study how the ECM participates in the motility of the δ-proteobacterium *Myxococcus xanthus*. *Myxococcus* cells move on solid surfaces both by A and S motility. S motility results from

Author contributions: A.D., M.-P.V., T.M., and O.T. designed research; A.D., M.-P.V., F.M., and O.T. performed research; A.D., M.-P.V., T.M., and O.T. analyzed data; and A.D., M.-P.V., T.M., and O.T. wrote the paper.

The authors declare no conflict of interest.

This article is a PNAS Direct Submission.

Freely available online through the PNAS open access option.

[1]A.D. and M.-P.V. contributed equally to this work.

[2]To whom correspondence may be addressed. E-mail: tmignot@ifr88.cnrs-mrs.fr or olivier.theodoly@inserm.fr.

This article contains supporting information online at www.pnas.org/lookup/suppl/doi:10.1073/pnas.1120979109/-/DCSupplemental.

polar retractile type IV pili acting as grappling hooks to pull the cell forward (5). A motility, otherwise called "gliding" motility, has not been understood for a long time. Gliding cells deposit an ECM slime, a mucus that becomes visible as a poorly contrasted white deposit in the wake of motile bacteria. It has been proposed that slime secretion could be directly responsible for gliding motility and may propel the cells if it were secreted selectively at the back of the cells (6). In this process, the slime polymer, a probable polysaccharide, would swell upon encounter with the aqueous phase of the extracellular milieu pushing the cell body in a ratchet-like manner (6). This model has recently been challenged by the discovery of the Agl/Glt machinery composed of an Agl internal molecular motor that exerts traction forces directly against the substrate through a large Glt envelope-spanning transducing complex (7, 8). In principle, *Myxococcus* gliding motility is thus similar to apicomplexan gliding motility (7). However, the role of slime has never been addressed directly, leaving its propulsive contribution as an open question. Slime could also facilitate motility, promoting specific adhesion and allowing cell–cell communication through the deposition of signaling molecules (2). In the past, slime has been observed by invasive techniques such as EM, nonspecific staining, or DIC on glass (6, 9) (see below), which prevented its analysis during the motility of live cells.

To address this limitation, we developed an assay to image slime secretion in real time by Wet-SEEC. We successfully quantified slime thickness and the rate of secretion during movement at unprecedented resolution, revealing that slime does not contribute to propulsion. Combined Wet-SEEC and fluorescent staining approaches showed that slime is deposited underneath the cell body at seemingly constant rates where it preferentially associates with the Agl/Glt motility motors. In doing so, slime provides specific adhesion sites for the motility complexes allowing the machinery to push on the substratum locally and produce thrust. This Wet-SEEC analysis thus elucidates a function of slime previously uncharacterized in bacterial motility and shows the power of the Wet-SEEC system to image and elucidate the function of nanometer-sized biological objects.

Results

Wet-SEEC Microscopy. Wet-SEEC microscopy (Fig. S1*A*) uses a conventional inverted microscope with episcopic illumination and specific substrates, called wet-surfs, in place of usual glass coverslides or plastic culture flasks. Wet-surf substrates are designed to optimize the contrast under convergent illumination of thin films immersed in solution, the contrast C being defined as the relative difference between the reflected intensity on the film I_F and on the bare surface I_S, $C = (I_F - I_S)/(I_F + I_S)$. Wet-surfs are fabricated from standard glass coverslides on which a coating of transparent inorganic oxide multilayer is used to set the reflection properties (*Materials and Methods*). Fig. 1*A* reports the calculated contrasts versus thickness on glass and on wet-surf coverslides for thin films of refractive index $n = 1.5$. In the 0- to 20-nm range, the theoretical contrast on glass is almost null, whereas on wet-surf, the contrast increases sharply with the thickness and approaches its maximum value of 1 at around 20 nm. Practically, considering that the eye has a contrast sensitivity limit of $C = 0.002$, wet-surf displays a 100-fold higher sensitivity with a 0.2-nm detectable minimal thickness versus 20 nm on glass.

To test the accuracy of the calculations, we constructed a series of resin thin films (*Materials and Methods*) whose thickness and refractive index were experimentally determined by atomic force microscopy (AFM) and ellipsometry. As observed in Fig. 1*B*, the theoretical and experimental reflected intensities from different thicknesses match perfectly, requiring no fitting parameter and validating our modelization. Hence, the precision of our calculation, combined with the sharp changes of contrast and intensity versus film thickness, should allow absolute measurement of thin film thickness and 3D reconstructions of samples topographies. Consistent with this property, we compared Wet-SEEC topographies of microfabricated resin stripes (Fig. 1*C*) with AFM measurements and found a 1-nm consistency in the vertical scale. To show that Wet-SEEC can be used to image biological specimens, for example a lipid bilayer, we prepared giant unilamellar dioleoyl phosphatidylcholine (DOPC) vesicles and imaged them after letting them sediment by gravity directly on a wet-surf, where they adhered, spread, and eventually burst, yielding a DOPC lipid bilayer settling on the substrate. On the Wet-SEEC image, the contrast between the bilayer and the bare substrate is sharp and

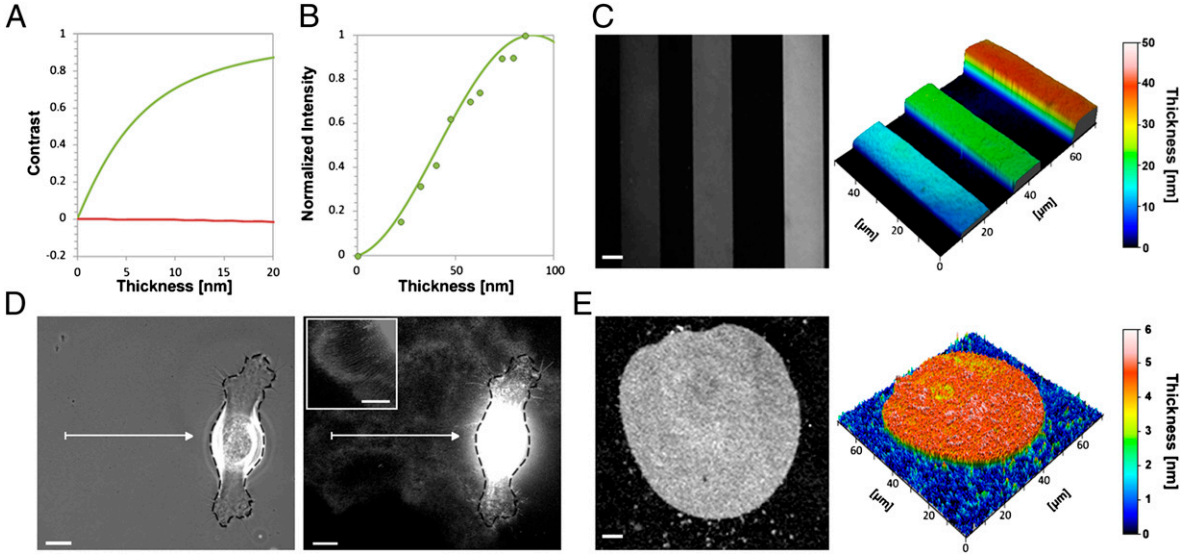

Fig. 1. Wet-SEEC imaging and topographic reconstructions of nanometer-size transparent layers. (*A*) Contrast calculations for a film of optical index $n = 1.5$ on a glass slide (red) and on a wet-surf (green) as a function of film thickness. (*B*) Wet-SEEC optical signal intensity as function of film thickness. Theoretical (solid line) and experimental (dots) normalized intensities on a wet-surf for thin resins films of optical index $n = 1.6$. (*C*, *E*) Raw Wet-SEEC image (*Left*) and Wet-SEEC topographic reconstruction (*Right*) of (*C*) the calibrated resin steps, with thicknesses of 10, 18, and 40 nm (from left to right) were measured in *B*, and (*E*) a DOPC lipid bilayer of 4.5 nm thickness. (*D*) Phase contrast, and Wet-SEEC images of ECM deposition in the wake of a motile keratinocyte cell. Dark dashed line represents the cell contour. (*Inset*) Tubular structures at cell proximity. (Scale bar, 10 μm.)

allows a topographic 3D reconstruction of the layer, showing an average thickness of 4.5 ± 0.5 nm (Fig. 1*E*), which is consistent with literature data (10). Finally, to test whether Wet-SEEC can be used to study instantaneous live cell processes, we imaged the complex matrix deposited by migrating keratinocytes on a fibronectin-functionalized wet-surf. In the past, this matrix consisting of a complex polysaccharide layer and what appears to be elongated lipid nanotubes, has only been observed by electron microscopy and specific fluorescence staining (11). On wet-surfs, the structural details of the keratinocyte ECM were readily observed: light zones were consistent with the described proteoglycan layers and darker patterns likely corresponded to the lipid nanotubes (Fig. 1*D*).

Direct Measurement of *Myxococcus* Slime Trails Thickness by Wet-SEEC. Standard *Myxococcus* gliding assays are conducted on agar (6). However, on this substrate slime is only detected at very low contrast (Fig. S1*B*) and the viscosity and variable thickness of agar make this substrate inappropriate for fluorescence staining or Wet-SEEC studies, blocking any slime quantitative studies on agar. As an alternative, slime was previously imaged by DIC directly on a glass coverslip (9). This technique improved the imaging of slime, which appeared as thin filaments attached to the cell body but it required transferring the cells from a culture well to a glass coverslip, which not only was invasive but also prevented the study of slime deposition during movement as *Myxococcus* cells do not glide on naked glass. To resolve these issues, we developed a microfluidic chamber and a glass substrate functionalized with chitosan, a linear polysaccharide composed of randomly distributed β-(1,4)-linked D-glucosamine (deacetylated unit) and *N*-acetyl-D-glucosamine (acetylated unit). The chitosan surface was perfectly regular and *Myxococcus* cells attached and moved at normal velocities despite the liquid phase (Fig. S1 *D* and *E* and Movie S1). Under these conditions, phase contrast or DIC imaging completely failed to detect slime deposited by chitosan-motile cells (Fig. 2*A*, *Left* and Movie S1). Strikingly, slime was detected at high contrast in the wake of motile bacteria when imaged by Wet-SEEC (Fig. 2*A*, *Right* and Movie S2). Surprisingly, slime was not continuous as suggested by low-resolution phase contrast images of agar-motile bacteria (6) (Fig. S1*B*) but presented extended continuous segments separated by patchy and scattered deposits (Fig. 2 *A* and *C* and Fig. S2). Absolute 3D-thickness topography could be computed and slime thickness was estimated to range between 0 and 5 nm with widths between 200 and 900 nm (Fig. 2 *B* and *C* and Fig. S2). Therefore, slime is up to 1,000-fold thinner that the bacterial cell (Fig. 2*D* and Movie S3), revealing the power of Wet-SEEC to detect extremely tenuous dynamic biological nanofilms.

Slime Is Deposited Underneath the Cell Body and Does Not Mediate Propulsion. If slime extrusion at the rear pole of the cell creates propulsion thrust, this thrust must overcome the drag force exerted by the viscous fluid surrounding the bacteria (6). In this case, the drag force would increase linearly with velocity and thicker slime regions should be correlated to high velocity phases, whereas the thinner and scattered deposits should match low-velocity phases. Contrary to this prediction, Wet-SEEC measurements of dynamic slime deposition revealed that slime is thicker at areas where the cells move slower (Fig. 3*A*). In fact, there was a clear correlation between the amounts of slime deposit and the time spent by a cell at given positions (Fig. 3*A*). These results suggest that slime is deposited at constant rates underneath the cell body.

DIC imaging of slime secretion by A-motility mutants suggested that these mutants secrete slime from both cell ends, which was proposed to explain their defect in motility (9). To test this possibility in a definitive way, we analyzed slime deposition by nonmotile cells (A^-S^-) carrying structural mutations in both type IV pili and the Agl/Glt system. When *pilA aglQ* and *pilA gltD/E* cells were allowed to settle on the substratum, they were nonmotile as expected but no slime deposition emanating from the poles was detected (Fig. 3*B*). To test whether these cells deposited slime underneath the cell body, the cells were flushed at different times. Slime was deposited underneath the cells and its thickness was directly correlated to the time spent on the chitosan substratum (Pearson coefficient = 0.61) (Fig. 3*B* and Fig. S3*A*). Furthermore, in all cases, slime was detected all over the area occupied by the cell body, arguing that slime is not secreted at the back of cells but seems distributed all over the cell envelope (Fig. 3*B* and Fig. S3*B*). Carbonyl cyanide-m-chlorophenylhydrazone (CCCP)-treated cells also deposited slime when they stopped, showing that the secretion pattern of A^-S^- cells does not result from the mutations that render cells nonmotile (Fig S3*C* and *SI Text S1*).

Finally, a potential caveat with these experiments is that slime may contain several components, among which capsular EPS (exopolysaccharides) or LPS, which may also be detected by Wet-SEEC and thus mask the bona fide motility slime. In *Myxococcus*, distinct capsular EPS have been shown to cover the cell surface of vegetative cells and spores (12, 13). In each case, EPS export to the cell surface requires a Wza-like outer membrane efflux channel (14). To test whether the Wet-SEEC slime is composed of capsular polysaccharides, we constructed a *wza*^{0}

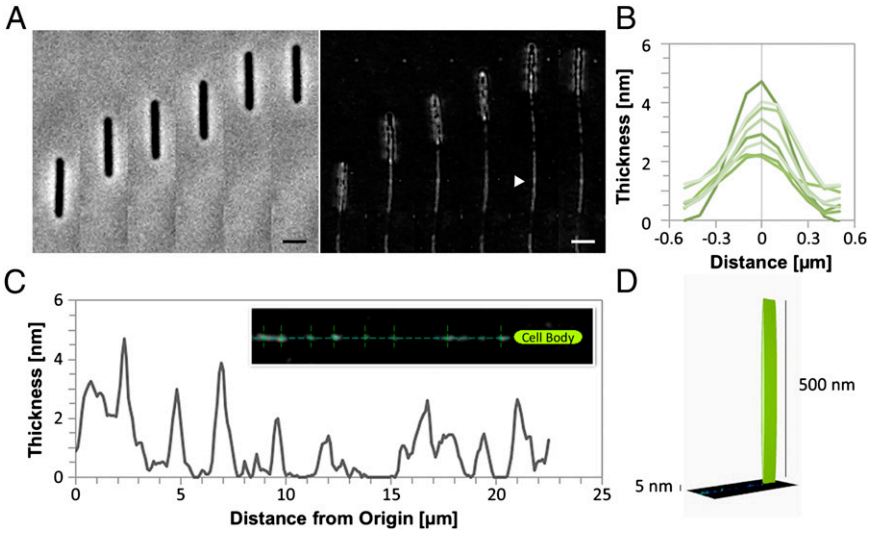

Fig. 2. Direct observation and topographic measurement of the *Myxococcus* slime trails by Wet-SEEC. (*A*) Phase contrast and Wet-SEEC images of slime deposition in the wake of a motile cell shown at different time points (for animation see Movie S2). Pictures were taken every 30 s. Triangle arrow points to the slime trail. (Scale bar, 1 µm.) (*B* and *C*) Longitudinal (*B*) and lateral (*C*) profiles of the slime trail given in the *Inset* of *B* showing local measured thickness (nanometers) (for animation, see Movie S3). (*D*) Schematic representation of the scale between the size of the cell body (500 nm of diameter) and the maximum slime thickness (5 nm).

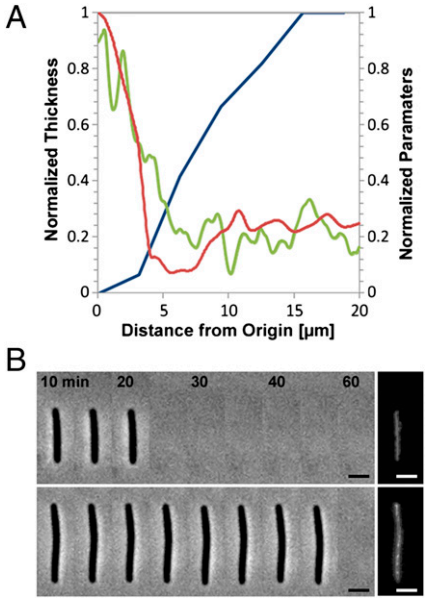

Fig. 3. Slime is deposited at constant rates underneath the cell body and does not mediate propulsion. (*A*) Slime thickness (green line) against cell velocity (blue line) or time residence at given locations (red line). Thickness, cell velocity, and residence were computed and normalized as discussed in *Materials and Methods*. (*B*) Slime deposition by mutant nonmotile cells. Cells were allowed to settle on the substratum and flushed at different times. Slime deposition underneath the cell body was observed after flushing using Wet-SEEC. (*Upper* and *Lower*) Two representative cells harboring different times of contact with the substratum. (Scale bar, 1 μm.)

mutant, in which all of the known and putative capsular EPS export machineries (*epsY*, *fdgA*, and MXAN1915) are knocked out (*SI Materials and Methods*). The *wza*^{0} mutant still moved on chitosan and deposited slime trails with no obvious alterations (Fig. S4 *A–C*). Furthermore, a *difA* mutant well known to lack capsular EPS (15) and a *sasA* mutant described to lack LPS-O-antigen, the surface-exposed portion of LPS (16) also deposited slime trails (Fig. S4 *C–E*). Therefore, although we cannot exclude that the motility slime also contains EPS and LPS-O-antigen, the results suggest that the main component of slime must be an additional unidentified polymer(s). Altogether, the results show that slime is deposited at seemingly constant rates underneath the cell body both by motile and nonmotile cells ruling out slime propulsion in a definitive manner.

Slime Mediates Adhesion and Is Deposited by the Motility Complexes During Motility. Could slime mediate adhesion of the motility machinery? The above results show that slime is still secreted by *aglQ* motor and *glt* transducer mutants, indicating that it is not secreted by the Agl/Glt machinery. However, it remains possible that the machinery uses the surface slime for its attachment, for example by recruiting it to its tip at the cell surface. Indeed, indirect evidence suggests that slime promotes adhesion to the substrate (*SI Text S2* and Fig. S5).

To elucidate the mechanism of slime deposition in a definitive manner, we developed a technique to visualize how slime is transferred from the cell body to the substrate. Because slime is likely a Wza export-independent polysaccharide, we took advantage of the chitosan system to screen fluorescent-derived lectins that would stain slime trails (Table S1). One of them, Concanavalin A (ConA) that selectively recognizes internal and nonreducing terminal α-D-mannosyl or α-D-glucosyl groups, bound both the cell body and the slime trails. Comparison of the ConA-staining patterns with slime on Wet-SEEC images revealed similar profiles, showing that both methods detect the same deposit which therefore must contain a polysaccharide or a glycoconjugate (glycoprotein or glycolipid) component (Fig. S6). ConA staining also stained slime in the *wza*^{0}, *difA*, and *sasA* mutants, confirming that the lectin stains the Wet-SEEC detected slime (Fig. S4).

On cells, ConA staining was not uniform but often covered the whole cell body with additional conspicuous bright dots distributed at regular intervals on the cell body (Fig. 4*A*). Strikingly, these dots often appeared at the leading cell pole and remained fixed, relative to the substratum before they eventually became deposited on the substratum (Fig. 4*A* and Movie S4). Thus, during motility, slime is locally concentrated and deposited underneath the cell body at fixed sites, explaining the regularity of the patches. The dynamics of slime clusters at the cell surface strongly suggests that slime is enriched and trafficked by the Agl/Glt system directly. To further test this hypothesis, we imaged slime cluster dynamics in immobile cells (*Materials and Methods* and ref. 7). In these cells, the Agl/Glt complex is not attached to the substratum and therefore does not remain static but is transported down the cell axis by the activity of the Agl motor (7). Thus, if slime clusters are attached to the tip of the motility machinery, they would also be expected to travel along the cell surface in immobile cells. Consistent with this assumption, moving slime clusters were observed in immobile cells and moved at speeds comparable to those measured for the motility complex (7) (Fig. 4*B* and Movie S5). Finally, to test directly whether slime is "pasted" by the machinery onto the chitosan substrate, we imaged ConA-stained slime and the Agl/Glt complexes using a two-color *Myxococcus* strain expressing labeled Agl/Glt components (AglQ-mCherry and AglZ-YFP) (7). In this experiment, we first monitored the positions of AglQ-mCherry and AglZ-YFP clusters in a gliding cell and injected ConA after the cell had left these positions to test where slime had been deposited. As previously described, colocalizing fixed AglQ-mCherry and AglZ-YFP clusters were readily observed along the cell body (Fig. 4*C*). ConA-stained slime patches were observed at the same positions, strongly suggesting that slime is associated with the motility machinery (Fig. 4*C*). Altogether, these results indicate that the machinery tip interacts with slime and deposits it directly on the substrate, promoting/reinforcing its adhesion to the substrate.

Discussion

Strategies to characterize molecular depositions on solid–liquid substrates are based on techniques that are invasive (transmission electron microscopy), slow (AFM), or using potentially perturbing additives (fluorescence microscopy). In this context, we have developed the Wet-SEEC method allowing the simultaneous observation of living cell behaviors and nanometric substrate details. We compared Wet-SEEC and more traditional fluorescent lectin-stained ECM tracks deposited by motile Myxobacteria, which revealed that Wet-SEEC detects all of the lectin-stained species. Therefore, the Wet-SEEC method is widely suitable for a range of biological organisms provided that an appropriate surface treatment is applied to the wet-surfs. The outmost surface of wet-surfs is made of silica and all standard surface treatments of glass coverslips are readily applicable on wet-surfs. In this work, we used fibronectin and chitosan to promote adhesion and motility of keratinocytes and *Myxococcus* on wet-surfs. In both cases, we observed the deposited ECM at unprecedented contrast. It should be noted however, that Wet-SEEC is not only applicable for cell surface interaction studies, but may also be used to image any nanosized biological object simply settled on a wet-surf, for example, a virus or a subcellular organelle (i.e., a vesicule). Finally, a potent asset of the technique is its easy integration into other microscopy techniques, including phase contrast, DIC, fluorescence, microfluidics, and total internal reflection fluorescence, allowing specimen imaging in multiple and complementary modes. This versatility makes Wet-SEEC applicable to a wide range of live applications, from simple observations to dynamic studies.

We used the Wet-SEEC method to characterize the poorly defined function of slime secretion by gliding Myxobacteria, which has been observed for more than three decades. Detailed slime studies have been greatly hampered by the inability to

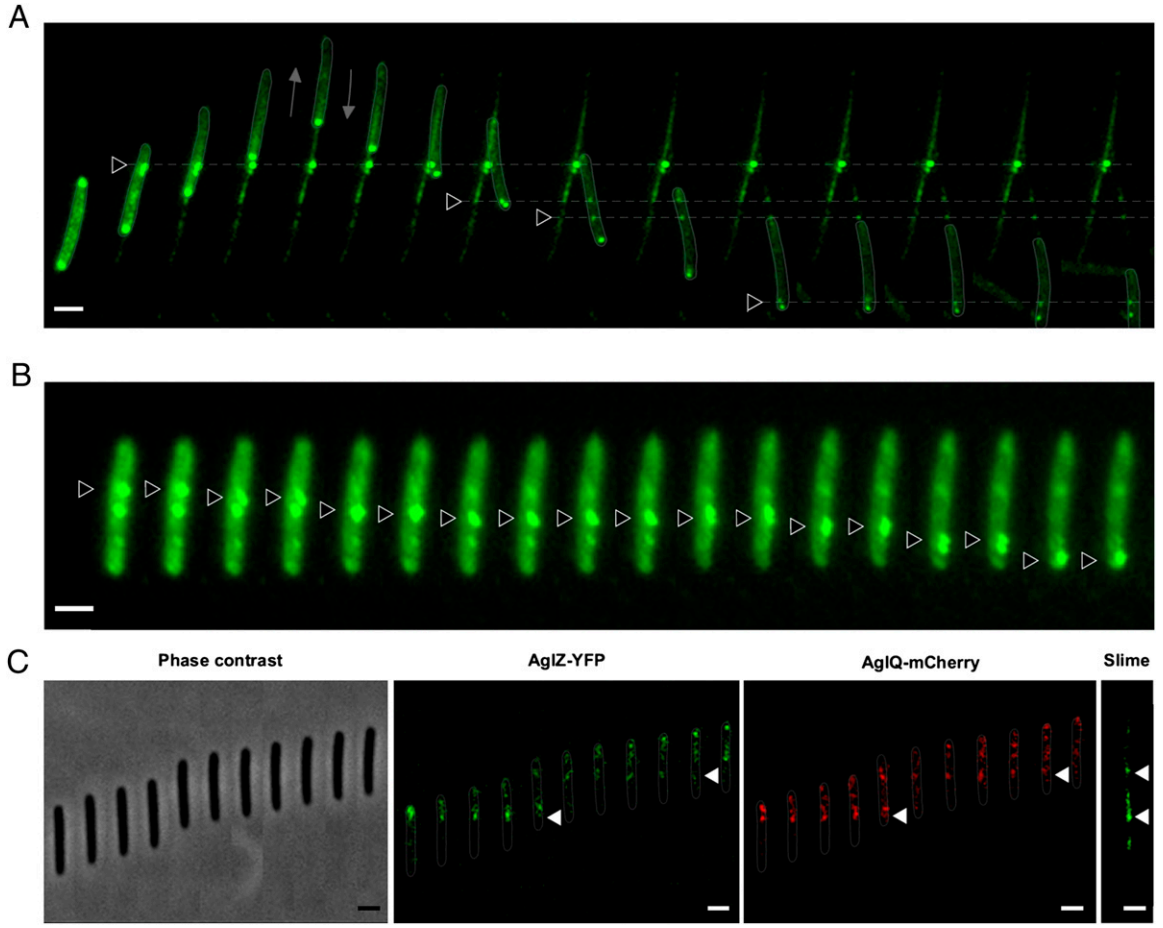

Fig. 4. Slime is deposited by the Agl/Glt motility complexes. (*A*) ConA staining of a moving cell and its resulting slime trail at different times. Note that the cell changes direction after t5 (2 min). Triangular arrows point to conspicuous bright dots that appear at the leading cell pole and remained fixed relative to the substratum before they eventually became deposited on the substratum (for animation, see Movie S4). Fluorescent micrographs were taken every 30 s. (Scale bar, 1 μm.) (*B*) ConA clusters are transported down the cell body in immobile cells. Two ConA bright clusters (black triangles) are shown to move down the cell axis. Pictures were taken every 15 s. (Scale bar, 1 μm.) (*C*) Slime patches are deposited where the Agl/Glt machinery assembles. Time lapse of a cell expressing both AglZ-YFP and AglQ-mCherry is shown. Phase contrast and corresponding YFP and mCherry micrographs are shown. Slime was stained with ConA after the cell left the positions shown on the *Left*. Triangular arrows point to fixed AglZ- and AglQ-bright motility complexes at positions where conspicuous slime patches were deposited. Fluorescent micrographs were taken every 15 s. (Scale bar, 1 μm.)

visualize the low contrast nanometer-sized slime polymer under native live conditions. Knowledge of the fine structure of slime was only obtained by electron microscopy on fixed cells, which revealed that slime is structured into seemingly coalescing ribbons emanating from underneath the cell body (6). However, how slime actually becomes deposited remained unclear. Using Wet-SEEC, it was possible to observe that slime is not continuous and contains scattered patches of variable thickness ranging between 0 and 5 nm, more than 250-fold thinner than the cell body itself. To our knowledge, this is a unique observation of a biological film of thickness below 5 nm by optical microscopy.

Combined Wet-SEEC analysis of slime and Concanavalin-A staining allowed us to elucidate how slime is deposited during motility, which revealed that slime is deposited at seemingly constant rate underneath the cell body and not from polar regions. This was most evident in motility mutants and CCCP-treated cells where slime was secreted underneath the cell body and not at both cell poles (9). This discrepancy with the Yu and Kaiser study (9) may be explained by the limits of their method, which required transferring the cells to a glass coverslip for microscopy and was therefore prone to manipulation artifacts. This study uses characterized *agl* and *glt* mutants (7, 8) and thus uniquely establishes the slime secretion patterns of structural A-motility machinery mutants, showing that slime export to the cell surface and global deposition do not require an active Agl/Glt machinery.

Slime secretion does not mediate propulsion but likely facilitates motility-driven attachment to the substrate. Two main lines of evidence suggest that propulsion cannot be due to an additional polymer, invisible by the Wet-SEEC method: (*i*) a *wza*^{0}/*sasA* mutants still deposit slime, showing that capsular polysaccharides and LPS-O-antigen may only constitute a minor component of the Wet-SEEC detected slime; and (*ii*) ConA-staining largely overlaps with the Wet-SEEC signal and is also detected in the *wza*^{0}/*sasA* mutants, showing that Wet-SEEC indeed detects the main slime sugar polymer. During motility, the slime deposition pattern is the "fingerprint" of the Agl/Glt motility machinery, suggesting that the pushing action of the motility machinery deposits slime on the substrate by a "paste-release" mechanism. An as yet unidentified terminal machinery component must have evolved affinity for slime to increase its local concentration at the machinery tip and improve machinery adhesion to the substrate. This way, the machinery itself may lay its own adhesion substrate, enhancing *Myxococcus* substrate adhesion and allowing cells to glide on a larger range of substrates.

Remarkably, self-deposited slime polymers seem a hallmark of gliding organisms: in prokaryotes, in myxococcales (6, 17), cyanobacteria (18), and bacteroidetes (19) and also in eukaryotes, in

apicomplexa (20, 21) and diatoms (22). Until now, the role of slime in gliding has been mostly studied in apicomplexa and diatoms and shown to contain adhesive macromolecules, proteins, and proteoglycans (21–23). In apicomplexa, slime contains thrombospondin-related anonymous protein (TRAP), an adhesive external component of the motility machinery. During motility, TRAP is released from the cell surface by proteolysis at the back of the parasites supporting forward movement; the deposition of surface-bound ConA-bright clusters by *Myxococcus* cells clearly suggests a TRAP-like adhesion-release mechanism in *Myxococcus* gliding (21). Hence, the deposition of adhesion-promoting polymers may be a conserved principle in gliding organisms.

In the future, it will be necessary to characterize the composition of slime and how it is recognized by the tip of the motility machinery. Slime is not a capsular Wza-exported EPS species. Comparison of Wet-SEEC and ConA staining images reveal that ConA recognizes the main slime component, suggesting that slime constitutes an as yet unidentified surface polysaccharide. Lipopolysaccharide, the major component of the bacterial outer membrane, is an attractive candidate because it contains α-mannosyl groups (recognizable by ConA) and covers the entire cell surface. Because LPS is essential to cell viability, *lps* mutants could not be tested; however, LPS-O-antigen mutants have been described (16) and still deposit slime (Fig. S4*D*). Finally, adhesion may not be the sole function of slime. It has long been known that *Myxococcus* cells can follow previously laid slime trails (17), suggesting that slime recognition is also a form of cell–cell communication. Trail following could well be driven by the machinery itself, which could preferentially engage existing slime patches.

Materials and Methods

Wet-SEEC. The Fresnel coefficients R_p and R_s of wet-surfs are optimized to achieve antireflective conditions in reflection microscopy assuming a conical illumination (angle of incidence θ ranging from 0 to θ_{max}). Calculations are performed for either unpolarized light (minimization of $\int_0^{\theta_{max}}(|R_p|^2+|R_s|^2)\sin\theta d\theta$) or crossed-polarized light (minimization of $\int_0^{\theta_{max}}|R_p+R_s|^2\sin\theta d\theta$) (24, 25). In this work, we used wet-surfs optimized for a wavelength λ = 550 nm and an illumination numerical aperture INA = 0.7 corresponding to θ_{max} = 30°. Microscopy images were recorded with a Zeiss axiovert 200 inverted microscope (Carl Zeiss) equipped with adjustable field and aperture stops. A differential interference contrast objective (plan-Apochromat 63 × 1.40 oil) and a reflection interference contrast microscopy objective (Zeiss Neofluar 63/1.25 antiflex) were used for respectively unpolarized light and crossed-polarized light images. Acquisition was taken with a CCD camera (Coolsnap HQ2; Photometrics) and a mercury lamp source (X-cite 120Q lamp), coupled to a narrow bandpass filter (λ = 546 nm ± 12 nm). Wet-surfs were fabricated from standard glass coverslides coated with a multilayer of inorganic oxides and display a silicon oxide top layer to approach surface physicochemical properties of standard glass coverslides. Wet-surfs have been designed to optimize the contrast under convergent illumination of a 1-nm-thick film of refractive index 1.5 immersed in solution. They were developed in collaboration with Nanolane and are now available commercially. For thickness measurement, the intensities *I* are normalized using the intensities of the bare substrate, I_0, and of a calibration resin step of thickness 15 nm, I_{15}:

$$I_N^i = \frac{I^i - I_{15}^i}{I_{15}^i - I_0^i},$$

where I_N, *is* the normalized intensity and the superscript i = e or i = t stands for experimental or theoretical. The normalized theoretical intensity dependence versus film thickness permits to invert experimental intensity images into 3D topographic reconstructions.

Microfluidic Experiments. Microfluidics straight channels of dimensions 20 μm × 50 μm × 4 mm were fabricated using standard soft lithography procedures (26). A positive mold was created by photolithography with SU-8 2050 negative resins (Microchem) on a silicon wafer (Siltronix). A replica was made with polydimethylsiloxane, PDMS (Sylgard 184 Silicone Elastomer Kit; Dow Corning). Ports to plug inlet and outlet tubings were punched with a gauge needle in the PDMS replica. The devices were finalized by sealing the PDMS piece on a wet-surf via O2-plasma activation (Harrick Plasma) of both surfaces. The chitosan-coating procedure was performed as follows. Briefly, channels were filled with 1 mL of chitosan (150 μg/mL) diluted in 2 M acetic acid. After incubation for 15 min at room temperature, the coating solution was removed by performing two successive washes with ultrapure water. Channels were then filled with the cell suspension previously washed and resuspended in TPM [10 mM Tris (pH 7.6), 8 mM $MgSO_4$, 100 mM KH_2PO_4] containing 100 mM of $CaCl_2$. Before the experiments, the flow cells were flushed with several milliliters of TPM $CaCl_2$ buffer to eliminate any nonadhering cells.

The primers (Table S2), plasmids (Table S3), and strains (Table S4) used in this study, keratinocyte cell line, and growth conditions as well as the procedures used for CCCP injections, lectin-staining, and time-lapse microscopy are further described in *SI Materials and Methods*.

ACKNOWLEDGMENTS. We thank Mélanie Sotes for the construction of the *Wza*° mutant; Clémentine Thibault for her help with Wet-SEEC and ConA experiments; Zhaomin Yang for the gift of HK1324; Yong Zhang for suggesting chitosan as a potential motility substrate; and Christophe Beloin, Emilia Mauriello, Sam Dukan, Thierry Doan, and Paul Amploi for discussions and critical reading of the manuscript. A.D. and part of this work were supported by Human Frontier Science Program Young Investigator Grant RGY0075/2008 (to T.M.). This work was performed in collaboration with the Nanolane company (Montfort le Gesnois, France), which fabricated the wet-surfs. The setup was partly funded by a grant from the "C-Nano Provence Alpes Côte d'Azur" network.

1. Wolf K, Friedl P (2011) Extracellular matrix determinants of proteolytic and non-proteolytic cell migration. *Trends Cell Biol* 21:736–744.
2. Shrout JD, Tolker-Nielsen T, Givskov M, Parsek MR (2011) The contribution of cell-cell signaling and motility to bacterial biofilm formation. *MRS Bull* 36:367–373.
3. Nomarski G (1955) Microinterféromètre differentiel à ondes polarisées [Differential microinterferometer using polarized light]. *J Phys Radium,* 16:9–S13. French.
4. Zernike F (1942) Phase contrast, a new method for the microscopic observation of transparent objects part II. *Physica* 9:974–986.
5. Wu SS, Kaiser D (1995) Genetic and functional evidence that Type IV pili are required for social gliding motility in Myxococcus xanthus. *Mol Microbiol* 18:547–558.
6. Wolgemuth C, Hoiczyk E, Kaiser D, Oster G (2002) How myxobacteria glide. *Curr Biol* 12:369–377.
7. Sun M, Wartel M, Cascales E, Shaevitz JW, Mignot T (2011) Motor-driven intracellular transport powers bacterial gliding motility. *Proc Natl Acad Sci USA* 108:7559–7564.
8. Luciano J, et al. (2011) Emergence and modular evolution of a novel motility machinery in bacteria. *PLoS Genet* 7:e1002268.
9. Yu R, Kaiser D (2007) Gliding motility and polarized slime secretion. *Mol Microbiol* 63: 454–467.
10. Erbe A, Sigel R (2007) Tilt angle of lipid acyl chains in unilamellar vesicles determined by ellipsometric light scattering. *Eur Phys J E Soft Matter* 22:303–309.
11. Kirfel G, Rigort A, Borm B, Schulte C, Herzog V (2003) Structural and compositional analysis of the keratinocyte migration track. *Cell Motil Cytoskeleton* 55:1–13.
12. Lu A, et al. (2005) Exopolysaccharide biosynthesis genes required for social motility in Myxococcus xanthus. *Mol Microbiol* 55:206–220.
13. Müller FD, Schink CW, Hoiczyk E, Cserti E, Higgs PI (2012) Spore formation in Myxococcus xanthus is tied to cytoskeleton functions and polysaccharide spore coat deposition. *Mol Microbiol* 83:486–505.
14. Dong C, et al. (2006) Wza the translocon for E. coli capsular polysaccharides defines a new class of membrane protein. *Nature* 444:226–229.
15. Xu Q, Black WP, Nascimi HM, Yang Z (2011) DifA, a methyl-accepting chemoreceptor protein-like sensory protein, uses a novel signaling mechanism to regulate exopolysaccharide production in Myxococcus xanthus. *J Bacteriol* 193:759–767.
16. Bowden MG, Kaplan HB (1998) The Myxococcus xanthus lipopolysaccharide O-antigen is required for social motility and multicellular development. *Mol Microbiol* 30: 275–284.
17. Burchard RP (1982) Trail following by gliding bacteria. *J Bacteriol* 152:495–501.
18. Hoiczyk E, Baumeister W (1998) The junctional pore complex, a prokaryotic secretion organelle, is the molecular motor underlying gliding motility in cyanobacteria. *Curr Biol* 8:1161–1168.
19. Pate JL (1985) Gliding motility in Cytophaga. *Microbiol Sci* 2:289–290, 293–295.
20. Kappe S, et al. (1999) Conservation of a gliding motility and cell invasion machinery in Apicomplexan parasites. *J Cell Biol* 147:937–944.
21. Morahan BJ, Wang L, Coppel RL (2009) No TRAP, no invasion. *Trends Parasitol* 25: 77–84.
22. Lind JL, et al. (1997) Substratum adhesion and gliding in a diatom are mediated by extracellular proteoglycans. *Planta* 203:213–221.
23. Sibley LD (2010) How apicomplexan parasites move in and out of cells. *Curr Opin Biotechnol* 21:592–598.
24. Ausserré D, Valignat M-P (2006) Wide-field optical imaging of surface nanostructures. *Nano Lett* 6:1384–1388.
25. Ausserré D, Valignat M-P (2007) Surface enhanced ellipsometric contrast (SEEC) basic theory and lambda/4 multilayered solutions. *Opt Express* 15:8329–8339.
26. Xia Y, Whitesides G (1998) Soft lithography. *Angewandte Chemie-International Edition* 37:551–575.